NIR to Visible Upconversion in Nanocrystalline and Bulk $Lu_2O_3:Er^{3+}$

Fiorenzo Vetrone, J. Christopher Boyer, and John A. Capobianco*

Department of Chemistry and Biochemistry, Concordia University, 1455 de Maisonneuve Blvd. W, Montreal, Canada

Adolfo Speghini and Marco Bettinelli

Dipartimento Scientifico e Tecnologico, Università di Verona, and INSTM, UdR Verona, Ca' Vignal, Strada Le Grazie 15, 37134 Verona, Italy

Received: January 28, 2002; In Final Form: April 4, 2002

In this paper we investigate the upconversion luminescence of bulk and nanocrystalline $Lu_{1.98}Er_{0.02}O_3$ following excitation into the $^4I_{11/2}$ level using 980 nm radiation. After NIR continuous wave excitation, blue, green, and red emissions were observed for both samples under investigation with the green emission dominating the upconversion spectrum. A power study reveals that the $^4S_{3/2}$ (green) and $^4F_{9/2}$ (red) emitting levels are populated via two-photon excited-state absorption (ESA) and energy-transfer upconversion (ETU) processes. Upconversion from the $^2P_{3/2}$ level is attained via a three-step phonon-assisted energy-transfer process. A marked temperature dependence of the excited-state lifetimes in both the bulk and nanocrystalline samples was evidenced.

1. Introduction

Lanthanide ions doped inorganic materials are particularly suitable for many applications, which involve the generation of artificial light. The emission of light from the lanthanide ions is due mainly to electric and magnetic dipole optical transitions within the $4f^n$ manifold or may also be of interconfigurational nature, involving configurations such as $4f^{n-1}5d$.[1] The outer, less energetic 5s and 5p shells shield the f-electrons from the influence of external forces and as a result, the intraconfigurational f−f emission spectra consists of relatively sharp lines.[2]

Toward the end of the 20th century and into the new millenium, there has been a renaissance in the study of lanthanide-doped powder phosphors. Modern day scientists are investigating the luminescence properties of these crystalline materials in the nanometer scale, with particle sizes under the 100 nm threshold.[3] These nanocrystals can be characterized by markedly different properties, compared to their bulk counterparts. The interest stems primarily from the fact that in some cases the luminescence efficiency is dependent on the size of the crystallite.[4] Thus, they are attractive for such applications as light-emitting diodes, photovoltaics, and even lasers.

An important process for the generation of visible light is near-infrared to visible upconversion. In this process, two (or more) low-energy photons from the excitation source are converted into one photon of higher energy.[5] The erbium ion (Er^{3+}) is ideally suited to convert infrared light to visible. It provides intermediate electronic energy levels ($^4I_{11/2}$ and $^4I_{13/2}$) with long lifetimes, which are easily accessible with near-infrared radiation and can be conveniently pumped with low-cost commercial diodes.[6]

The upconversion efficiency is governed principally by the nonradiative processes of the host material.[7] By carefully selecting the environment for the Er^{3+} ion, the dynamics of the excited states can be controlled resulting in a reduction of the multiphonon relaxation and thus producing efficient upconversion.

Rare earth sesquioxides, such as Y_2O_3 and Lu_2O_3, have enjoyed present-day resurgence as nanocrystals owing to their favorable physical properties (high melting point, phase stability, and low thermal expansion). Moreover, they possess relatively low phonon energies (phonon cutoff about 600 cm^{-1}),[8] which are favorable for the upconversion process. The Lu_2O_3 lattice crystallizes in a cubic bixbyite structure with space group Ia3.[9,10] Two distinct sites are available for the lanthanide ions, one with point-group symmetry C_2 and the other with C_{3i} symmetry.[11] The C_{3i} site has associated with it a center of inversion and therefore, according to the selection rules, electric dipole transitions are forbidden. It is then expected that f−f spectra exhibit electric dipole transitions pertaining mainly to the Er^{3+} ions in C_2 sites and magnetic dipole transitions from both sites.

In a previous paper, we have shown the emission and upconversion ($\lambda_{exc} = 804$ nm) spectra for bulk and nanocrystalline cubic Lu_2O_3 doped with 1 mol % Er^{3+}.[8] In this paper, we extend the study of the upconversion by examining the emission after excitation at 980 nm into the $^4I_{11/2}$ level.

2. Experimental Section

Lu_2O_3 nanocrystals doped with 1 mol % Er_2O_3 ($Lu_{1.98}Er_{0.02}O_3$) were prepared using a solution combustion (propellant) synthesis procedure.[12,13] Propellant synthesis is a novel technique capable of producing nanopowders at relatively low temperatures and in a timely manner. The process involves the exothermic reaction between a metal nitrate (oxidizer) and an organic fuel, such as glycine. The stoichiometric synthesis reaction is

$$6\,M(NO_3)_3 + 10\,NH_2CH_2COOH + 18\,O_2 \rightarrow 3\,M_2O_3 + 5\,N_2 + 18\,NO_2 + 20\,CO_2 + 25\,H_2O$$

where M is Lu and Er. The size of the nanopowders is greatly influenced by the reaction temperature, which can be controlled by adjusting the glycine-to-metal nitrate molar ratio.[13] We

* To whom correspondence should be addressed. Telephone: +1-514-848-3350. Fax: +1-514-848-2868. E-mail: capo@vax2.concordia.ca.

10.1021/jp020256m CCC: $22.00
Published on Web 05/14/2002

employed a glycine-to-metal nitrate molar ratio of 1.2:1 to prepare the aqueous precursor solution. After the synthesis, the resulting nanocrystalline material was fired at 500 °C for 1 h to decompose any residual nitrate ions. The particle size of the sample was determined to be about 50 nm by wide-angle X-ray scattering (WAXS).

For comparison, a bulk sample with identical Er^{3+} concentration ($Lu_{1.98}Er_{0.02}O_3$) was prepared by intimately mixing the oxides, Lu_2O_3 (Aldrich, 99.99%) and Er_2O_3 (Aldrich, 99.99+%), pressing the powders into pellets under 10 tons of pressure and firing them in air at 1500 °C for 24 h. At this temperature, the optimum homogeneity was obtained.

All lutetia samples were kept in air without any further precaution.

Direct luminescence spectra were obtained by exciting the samples at 488 nm using a Coherent Sabre Innova, 20 W argon ion laser. Upconversion spectra were obtained by exciting at 980 nm using a Spectra-Physics model 3900 titanium sapphire laser pumped by the 514.5 nm line of the Ar^+ laser. The visible emissions were collected and dispersed using a Jarrel-Ash 1-meter Czerny Turner double monochromator. A thermoelectrically cooled photomultiplier tube (Hamamatsu R943−02) was used to monitor the signal. A preamplifier (Stanford Research Systems, model SR 440) processed the PMT signals and a gated photon counter (Stanford Research Systems, model SR 400) data acquisition system was used as an interface between the computer and the spectroscopic hardware. The signal was recorded under computer control using the Stanford Research Systems SR 465 software data acquisition/analyzer system.

The decay times were obtained by modulating the excitation sources mentioned above using an optical chopper (Stanford Research Systems, model SR 540) and were recorded using a gated photon counter.

A continuous flow cryostat (Janis Research ST-VP-4) was used to acquire the low-temperature spectra, and a Lakeshore model 330 controller was used to monitor the temperature.

3. Results and Discussion

On excitation with 488 nm at room temperature, the Er^{3+} doped bulk and nanocrystalline Lu_2O_3 yield distinct emission bands because of the intra-configurational f−f transitions (Figure 1). Green emission was observed from the ($^2H_{11/2}$, $^4S_{3/2}$) → $^4I_{15/2}$ transition between 500 and 580 nm. Red emission was observed from the $^4F_{9/2} \rightarrow {}^4I_{15/2}$ transition between 640 and 690 nm. NIR emission was observed in the ranges 785−825 nm and 840−870 nm assigned to the $^4I_{9/2} \rightarrow {}^4I_{15/2}$ and $^4S_{3/2} \rightarrow {}^4I_{13/2}$ transitions, respectively.

The observed decay curves for the $^4S_{3/2} \rightarrow {}^4I_{15/2}$ and $^4F_{9/2} \rightarrow {}^4I_{15/2}$ transitions following 488 nm excitation were fitted using a single-exponential function (Table 1). The decay times for the nanocrystalline material are in general shorter than for the bulk, which could be attributed to a higher probability for multiphonon relaxation in the nanocrystalline material owing to the presence of contaminants on their surface. Lu_2O_3 can adsorb atmospheric CO_2 and H_2O;[8] in fact, the combustion process produces CO_2 and H_2O as byproducts of the synthesis reaction, which could therefore be adsorbed immediately after the formation of the nanoparticles. While the residual nitrate ions are decomposed after firing the nanocrystals at 500 °C for 1 h, as confirmed by the absence of their characteristic bands in the MIR and Raman spectra (not shown), we have evidence that the heat treatment did not completely remove either the carbon dioxide or water from the surface of the nanocrystals. In fact, as reported previously,[8] the MIR spectra of nanocrystalline Lu_2O_3, prepared by the method above, show bands occurring at approximately 1500 and 3350 cm^{-1}, assigned to vibrations of the carbonate and hydroxyl groups, respectively. The presence of these groups on the nanocrystalline surface yields higher energy vibrational quanta as compared to the phonons of bulk lutetia (phonon cutoff of about 600 cm^{-1}). In the nanocrystalline material, the presence of vibrational quanta of about 1500 and 3350 cm^{-1} makes multiphonon relaxation much more probable than in the bulk material, increases the rate of depopulation, and therefore gives rise to a shorter observed decay time with respect to the bulk sample.

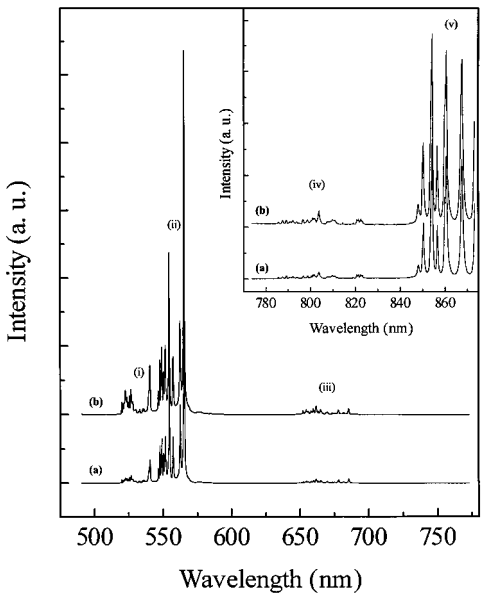

Figure 1. Room-temperature luminescence of (a) bulk and (b) nanocrystalline $Lu_{1.98}Er_{0.02}O_3$ following 488 nm excitation. (i) $^2H_{11/2} \rightarrow {}^4I_{15/2}$ (ii) $^4S_{3/2} \rightarrow {}^4I_{15/2}$ (iii) $^4F_{9/2} \rightarrow {}^4I_{15/2}$. Inset: (iv) $^4I_{9/2} \rightarrow {}^4I_{15/2}$ (v) $^4S_{3/2} \rightarrow {}^4I_{13/2}$.

TABLE 1: Room Temperature Decay Times for Bulk and Nanocrystalline Lu_2O_3:Er^{3+} Obtained from an Exponential Fit of the Decay Curves upon 488 and 980 nm Excitation

	decay time (μs)			
	bulk		nanocrystal	
transition	488 nm	980 nm	488 nm	980 nm
$^2H_{11/2} \rightarrow {}^4I_{15/2}$	63		53	
$^4S_{3/2} \rightarrow {}^4I_{15/2}$	62	190	55	246
$^4F_{9/2} \rightarrow {}^4I_{15/2}$	74	334	42	315
$^4I_{9/2} \rightarrow {}^4I_{15/2}$	61		47	
$^4S_{3/2} \rightarrow {}^4I_{13/2}$	63		54	

Excitation of bulk and nanocrystalline Lu_2O_3 with NIR light (λ_{exc} = 980 nm) into the $^4I_{11/2}$ level of the Er^{3+} ion produced intense upconversion luminescence spectra (Figure 2). Blue upconversion was observed with bands centered at 460, 475, and 495 nm, which are assigned to the $^4F_{5/2} \rightarrow {}^4I_{15/2}$, $^2P_{3/2} \rightarrow {}^4I_{11/2}$, and $^4F_{7/2} \rightarrow {}^4I_{15/2}$ transitions, respectively. Similar to the direct emission spectra, upconverted green emission was observed from the thermalized $^2H_{11/2} \rightarrow {}^4I_{15/2}$ and $^4S_{3/2} \rightarrow {}^4I_{15/2}$ transitions centered at 525 and 550 nm, respectively. Upconverted red emission centered at 660 nm was assigned to the $^4F_{9/2} \rightarrow {}^4I_{15/2}$ transition. The bulk and nanocrystalline samples exhibit a visually dominant green emission following 980 nm excitation ascribed to the spin-allowed $^4S_{3/2} \rightarrow {}^4I_{15/2}$ transition.

We have also observed NIR to visible upconversion in bulk and nanocrystalline Y_2O_3:Er^{3+} [14] and Lu_2O_3:Er^{3+} [8] following 800 nm excitation. The spectral features of yttria and lutetia bulk samples were similar save for a slight red shift (30 cm^{-1})

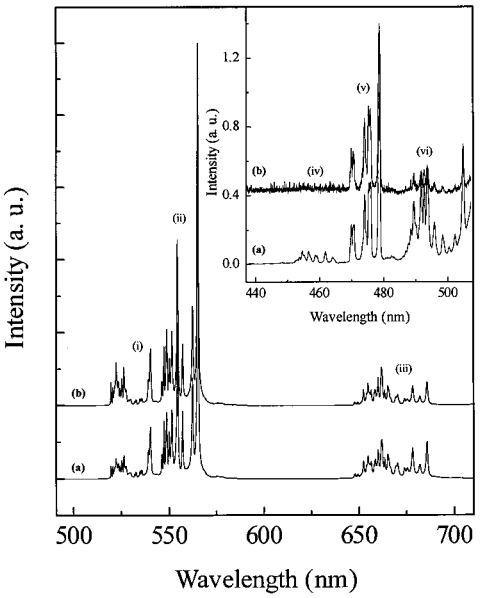

Figure 2. Room-temperature upconversion luminescence of (a) bulk and (b) nanocrystalline $Lu_{1.98}Er_{0.02}O_3$ following 980 nm excitation. (i) $^2H_{11/2} \rightarrow {}^4I_{15/2}$ (ii) $^4S_{3/2} \rightarrow {}^4I_{15/2}$ (iii) $^4F_{9/2} \rightarrow {}^4I_{15/2}$. Inset: (iv) $^4F_{5/2} \rightarrow {}^4I_{15/2}$ (v) $^2P_{3/2} \rightarrow {}^4I_{11/2}$ (vi) $^4F_{7/2} \rightarrow {}^4I_{15/2}$.

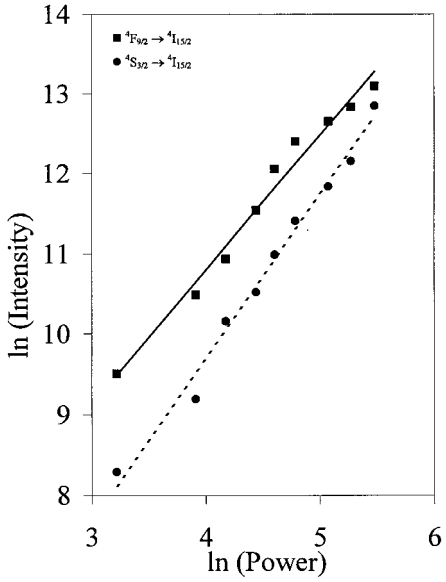

Figure 3. Power dependence of the green and red upconversion luminescence intensity of nanocrystalline $Lu_2O_3:Er^{3+}$ observed following 980 nm excitation.

in the $Lu_2O_3:Er^{3+}$ spectrum owing to different crystal field effects felt by the Er^{3+} dopant. However, striking differences are observed in the upconversion intensities between the two isostructural nanocrystalline samples. Under identical experimental conditions and dopant concentration, nanocrystalline $Lu_2O_3:Er^{3+}$ shows upconversion with luminescence approximately 10^2 times greater than $Y_2O_3:Er^{3+}$. In fact, in nanocrystalline $Y_2O_3:Er^{3+}$, no noticeable blue upconversion was observed. It has been observed that when comparing the emission properties of yttrium and lutetium containing oxide[15] and fluoride[16] crystals, the lutetium-based crystals show stronger luminescence. A possible explanation could be found on the basis of an intensity-borrowing mechanism mixing the 4f and 5d orbitals of the Ln^{3+} ion via the lattice valence-band levels, as proposed by Guillot-Noël et al.[17] In fact, in Y-based compounds, the valence-band energy levels are due predominantly to the oxygen or fluorine 2p orbitals, whereas in Lu crystals, the top of the valence band would be composed mainly of Lu 4f orbitals.[18] It follows that lutetium could be a more favorable cation than yttrium for trivalent lanthanide dopant emission.

The process by which the excited states are populated can be accomplished by several known mechanisms:[19−21] (i) excited-state absorption (ESA); (ii) photon avalanche (PA); and (iii) energy transfer (ETU). To better understand the mechanism by which the $^4S_{3/2}$ and $^4F_{9/2}$ levels are populated, the upconverted luminescence intensity I of the green ($^4S_{3/2} \rightarrow {}^4I_{15/2}$) and red ($^4F_{9/2} \rightarrow {}^4I_{15/2}$) transitions was measured as a function of the pump power P. The slope of the curve ln(I) versus ln(P) was 1.9 and 1.6, respectively (Figure 3), so we can therefore propose that two photons partake in the upconversion processes involved in the population of the $^4S_{3/2}$ and $^4F_{9/2}$ levels. Immediately, the PA mechanism was eliminated as a possible mechanism as no inflection point was observed in the power study.[22] In the PA mechanism, the upconverted luminescence is weak until a certain excitation density is achieved, after which, the emission becomes very intense and the behavior of ln(P) versus ln(I) exhibits a bending point. This is clearly not the case for either bulk or nanocrystalline $Lu_2O_3:Er^{3+}$. In the bulk and nanocrystalline material, upconversion can therefore only occur via an ESA or ETU process.

The ESA model involves only a single ion and it is usually the only upconversion process, which occurs in materials at low-dopant concentrations. In this process, an incoming photon from the pump beam will bring the ion already in an intermediate excited level ($|1>$) to an upper level ($|2>$). In the framework of the proposed model, the population N_2 of level $|2>$ is given by

$$N_2(t) = \frac{N_0 A_{01} A_{12} I^2{}_0}{\tau^{-1}{}_2(\tau^{-1}{}_1 + A_{12} I_0)} \qquad (1)$$

where N_0 is the initial population of the ion in the ground state ($|0>$), A_{ij} is a characteristic constant involving the oscillator strengths for the transitions from the initial state $|i>$ to the final state $|j>$. I_0 describes the density of photons in the pump beam while $\tau_1{}^{-1}$ and $\tau_2{}^{-1}$ are the intrinsic relaxation rates of levels $|1>$ and $|2>$, respectively. According to eq 1, the upconverted luminescence varies quadratically with the pump beam (I_0) but varies linearly with the concentration of the emitting particle.

Using the proposed model, one photon at 980 nm from the pump beam will excite the Er^{3+} ion from the $^4I_{15/2}$ ground state ($|0>$) to the $^4I_{11/2}$ intermediate excited state ($|1>$). A second photon of equal energy brings the ion to the $^4F_{7/2}$ level ($|2>$), which has an energy exactly twice that of the excitation pump beam (see Figure 4a). Multiphonon relaxation will then populate the $^2H_{11/2}$, $^4S_{3/2}$, and $^4F_{9/2}$ levels.

However, we cannot readily exclude the presence of the ETU mechanism acting in conjunction with the ESA process. In samples having a dopant concentration of 0.5 mol % or less, the energy transfer between dopant ions can be considered as negligible,[23] as the ions are too far apart and therefore the interaction with one another is very weak. The bulk and nanocrystalline samples used in this study have a dopant Er^{3+} concentration of 1 mol % and therefore, it is conceivable that the ETU process could be efficient. ETU proceeds according to a scheme in which two ions in close proximity are excited in an intermediate level $|1>$ and are coupled by a nonradiative process in which one ion returns to the ground state $|0>$ while

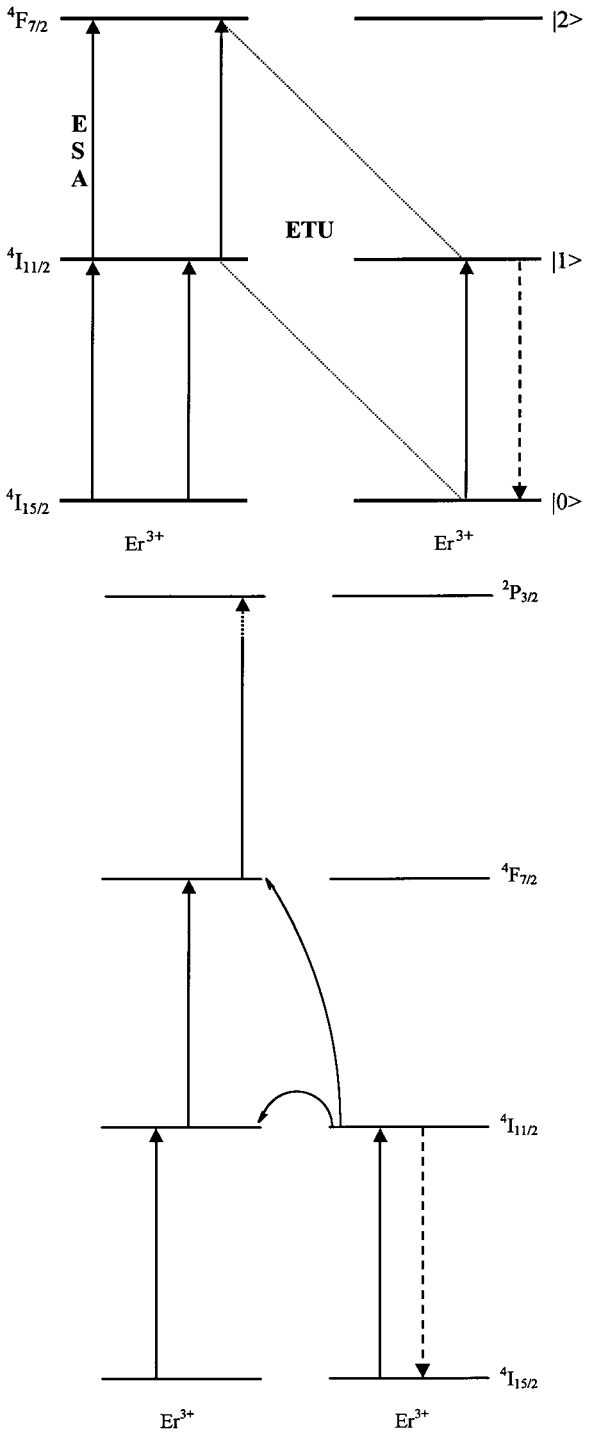

Figure 4. (a) Schematic representation of the ESA and ETU processes in bulk and nanocrystalline $Lu_2O_3:Er^{3+}$. (b) Schematic representation of the phonon-assisted ETU process in bulk and nanocrystalline $Lu_2O_3:Er^{3+}$ responsible for populating the $^2P_{3/2}$ level.

the other is promoted to the upper level |2>. Using the same symbols as above, population of level |2> can be written as

$$N_2(t) = \frac{(N_0 A_{01} I_0)^2 \sigma_u}{\tau_2^{-1} (\tau_1^{-1})^2} \qquad (2)$$

where σ_u is the rate constant for the ETU process. Similar to ESA, in the ETU process the population of level |2> varies quadratically with the density of photons in the pump beam (I_0) but, at variance with ESA, also varies quadratically with

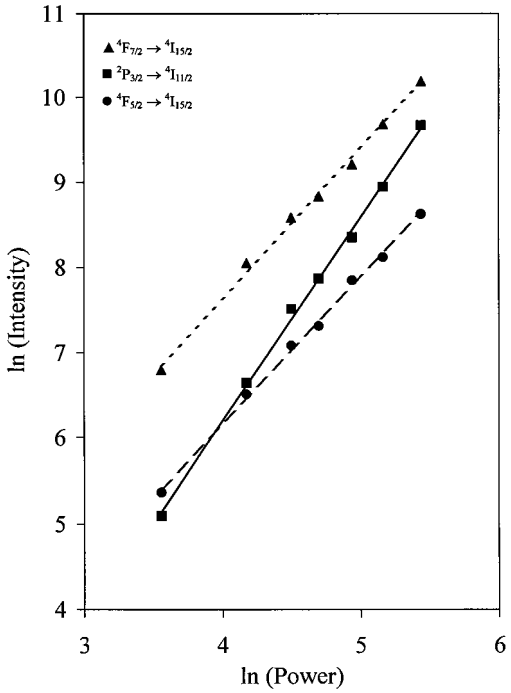

Figure 5. Power dependence of the blue upconversion luminescence intensity of bulk $Lu_2O_3:Er^{3+}$ observed following 980 nm excitation.

the dopant concentration N_0. Using the proposed model, the ETU process (see Figure 4a) occurs as follows: One Er^{3+} ion is excited to the $^4I_{11/2}$ level by the pump laser beam. A neighboring Er^{3+} ion also in the $^4I_{11/2}$ level transfers its energy to the initial ion thereby exciting it to the $^4F_{7/2}$ level while it returns to the ground state. Again, nonradiative phonon decay populates the green- and red-emitting levels.

Table 1 shows the room-temperature emission lifetimes of the $^4S_{3/2}$ and $^4F_{9/2}$ levels following excitation with 488 and 980 nm radiation. While the decay curves of the excited states following 488 nm excitation were exponential, the same is not true following 980 nm excitation, which showed a slight deviation from single-exponential decay. In the bulk and nanocrystalline samples, the decay times in the anti-Stokes emission ($\lambda_{exc} = 980$ nm) are significantly longer than the ones measured for the same states when exciting directly ($\lambda_{exc} = 488$ nm). Lengthening of the decay times following upconversion pumping is a clear indication of the presence of an ETU process.[24]

A power study was also performed on the blue-emitting levels of bulk $Lu_2O_3:Er^{3+}$. From the fitting of the ln(I) versus ln(P) curves for the $^4F_{7/2} \rightarrow {}^4I_{15/2}$ and $^4F_{5/2} \rightarrow {}^4I_{15/2}$ emission transitions, the slopes were 1.8 and 1.7, respectively (Figure 5), and therefore two photons partake in the upconversion processes involved in the population of the $^4F_{7/2}$ and $^4F_{5/2}$ levels. The $^4F_{7/2}$ level is therefore likely to be populated via an ESA or ETU process involving two photons of 980 nm, as described above (see Figure 4a). On the other hand, the $^4F_{5/2}$ level is approximately 1400 cm^{-1} higher in energy than the $^4F_{7/2}$ level and so for this level to be populated via two photons, a phonon-assisted process should be operative. Pure lutetia possesses a maximum phonon energy of approximately 600 cm^{-1} and therefore two or three phonons of such energy would be required to bridge the 1400 cm^{-1} energy gap, resulting in a phonon-assisted upconversion process. Moreover, as mentioned above, carbonate ions are adsorbed on the surface of the nanoparticles, and therefore one 1500 cm^{-1} phonon could possibly be involved as well in the phonon-assisted upconversion.

The slope of the ln(I) versus ln(P) curve for the $^2P_{3/2} \rightarrow {}^4I_{11/2}$ transition (shown in Figure 5) was 2.8, denoting that three photons were responsible for the upconversion process. In bulk $Y_2O_3:Er^{3+}$, we have studied the blue upconversion following 804 nm excitation as a function of the Er^{3+} concentration[14] and have shown that ETU and ESA mechanisms were operating simultaneously. In particular, it was observed that at low Er^{3+} concentrations (<1 mol %), the dominant mechanism is ESA, the reason being that the Er^{3+} ions are not very close to one another and the interionic interactions are very small. As the erbium concentration increases more and more, the interionic interaction increases and the ETU process becomes more and more important.

In the present case we excited at 980 nm and thus, the mechanism that we propose to be responsible for populating the $^2P_{3/2}$ level is slightly different. The Er^{3+} energy-level diagram reveals that there is no energy level, which could be populated by a sequential absorption of three pump photons. In fact, if the $^4F_{7/2}$ level is populated by the simultaneous absorption of two photons, (ESA mechanism, see Figure 4a), there is no energy level that could be populated by the absorption of another photon. Similarly, if the ion in the ground state is excited by one photon to the $^4I_{11/2}$ level and then nonradiatively decays to the $^4I_{13/2}$ level, a second photon has no resonant energy level for which to populate. Therefore, we propose a phonon-assisted ETU mechanism (Figure 4b), in which one to two maximum energy phonons are requested to compensate the mismatch in energy (approximately 690 cm^{-1}).

The upconversion spectrum obtained at 77 K (not shown) can be used to further illustrate that the population of the $^4F_{5/2}$ and $^2P_{3/2}$ energy levels can be caused by a phonon-assisted process. In fact, at 77 K, emission from the $^4F_{5/2}$ level is not observed while emission from the $^2P_{3/2}$ level is only barely detectable. This experimental evidence could be well explained by the proposed mechanisms required to populate the $^4F_{5/2}$ and $^2P_{3/2}$ levels. In the former mechanism, two to three lattice phonons are involved while one to two phonons are required for the latter one. Then, the decrease of the temperature induces a stronger decrease of the population of the $^4F_{5/2}$ level with respect to the $^2P_{3/2}$ level. Therefore, a corresponding decrease of the emission intensity of the $^4F_{5/2} \rightarrow {}^4I_{15/2}$ transition with respect to the $^2P_{3/2} \rightarrow {}^4I_{11/2}$ transition is observed.

The temperature dependence of the green and red upconversion luminescence for bulk and nanocrystalline $Lu_2O_3:Er^{3+}$ following 980 nm was studied. At 77K, transitions to the ground state originating from the $^2H_{11/2}$ level are not observed. However, as the temperature is increased to 298 K, we observed an increase in the luminescence intensity of the $^2H_{11/2} \rightarrow {}^4I_{15/2}$ transition and a decrease of the $^4S_{3/2} \rightarrow {}^4I_{15/2}$ intensity. This occurs because the $^4S_{3/2}$ level is the feeding level for the $^2H_{11/2}$ level and as a result of the population of the $^2H_{11/2}$ level, the $^4S_{3/2}$ level is depopulated. As the energy gap between the $^4S_{3/2}$ and $^2H_{11/2}$ levels is about 700 cm^{-1}, at room temperature both are populated while at 77 K, the thermalization is very small. The temperature dependence of the ($^2H_{11/2}$, $^4S_{3/2}$) $\rightarrow {}^4I_{15/2}$ transition in the nanocrystalline sample can be seen in Figure 6 (the bulk sample shows the same spectral temperature dependence). If we denote as A_1 and A_2 the experimental integrated luminescence intensities of the $^4S_{3/2} \rightarrow {}^4I_{15/2}$ and $^2H_{11/2} \rightarrow {}^4I_{15/2}$ transitions, respectively, the thermalization of the $^2H_{11/2}$ level may be expressed by the following equation:[25]

$$\frac{A_2}{A_1} = C \exp(-\Delta E/kT) \qquad (3)$$

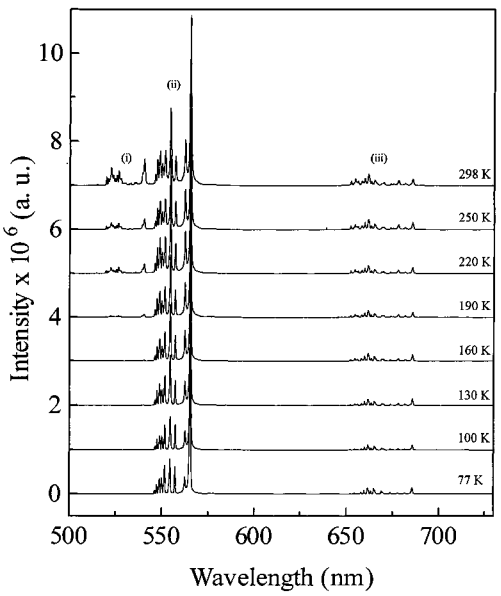

Figure 6. Upconversion luminescence spectra of nanocrystalline $Lu_2O_3:Er^{3+}$ at different temperatures ($\lambda_{exc} = 980$ nm): (i) $^2H_{11/2} \rightarrow {}^4I_{15/2}$, (ii) $^4S_{3/2} \rightarrow {}^4I_{15/2}$, and (iii) $^4F_{9/2} \rightarrow {}^4I_{15/2}$ transitions. The intensities of emission are normalized to the green ($^4S_{3/2} \rightarrow {}^4I_{15/2}$) transition.

TABLE 2: Decay Times for Bulk and Nanocrystalline $Lu_2O_3:Er^{3+}$ Obtained from an Exponential Fit of the Decay Curves for the $^4S_{3/2} \rightarrow {}^4I_{15/2}$ and $^4F_{9/2} \rightarrow {}^4I_{15/2}$ Transitions upon 980 nm Excitation at Various Temperatures

	$^4S_{3/2} \rightarrow {}^4I_{15/2}$ decay time (μs)		$^4F_{9/2} \rightarrow {}^4I_{15/2}$ decay time (μs)	
temperature (K)	bulk	nanocrystal	bulk	nanocrystal
77	414	447	423	692
100	372	406	415	664
130	349	393	409	628
160	311	381	400	575
190	277	353	389	553
220	254	339	373	540
250	226	266	352	450
298	190	246	334	315

where C is a constant, k is the Boltzmann constant, T is the absolute temperature, and ΔE is the energy gap separating levels $^4S_{3/2}$ and $^2H_{11/2}$. The calculated values of $\ln(A_2/A_1)$ as a function of $1/T$ were fitted using a straight line, and from the slope an energy gap of 689 cm^{-1} was obtained. This value is in good agreement with the difference between the lowest energy $^2H_{11/2}$ Stark level and the highest energy $^4S_{3/2}$ Stark level determined from the luminescence spectra ($\Delta E = 720$ cm^{-1}).

The decay curves of the upconverted green ($^4S_{3/2} \rightarrow {}^4I_{15/2}$) and red ($^4F_{9/2} \rightarrow {}^4I_{15/2}$) emissions were also measured as a function of temperature. Table 2 presents the decay times of the $^4F_{9/2}$ and $^4S_{3/2}$ levels versus temperature for both bulk and nanocrystalline $Lu_2O_3:Er^{3+}$.

The decay times of the $^4S_{3/2}$ and $^4F_{9/2}$ levels obtained by the upconversion process ($\lambda_{exc} = 980$ nm) are much longer than those obtained by direct excitation ($\lambda_{exc} = 488$ nm) for both bulk and nanocrystalline samples (see Table 1). This evidence could be explained by noting that both excitation processes populate the $^4F_{7/2}$ level, which in turn decays to lower levels. However, in the upconversion process, it could be assumed that the decays of the emitting levels reflect the feeding from longer-lived states.

Moreover, the decay times of the $^4S_{3/2}$ and $^4F_{9/2}$ levels are longer for the nanocrystalline sample with respect to the bulk sample. This peculiar behavior was evidenced and explained

for Eu^{3+} doped yttria by Meltzer et al.[26] In fact, the radiative lifetime of an electronic transition of an ion embedded in a medium was correlated with an effective refractive index n_{eff}, which is a function of the refractive index of yttria and the fraction of space occupied by the nanoparticles surrounded by the media with refractive index n_{med}. As the refractive index of lutetia is close to 2,[27,28] a value definitely higher than that of air ($n_{air} = n_{med} = 1$), a lengthening of the decay times of the electronic levels of Er^{3+} for the nanoparticles is expected, in agreement with the present results.

From Table 2, we observe that for both bulk and nanocrystalline samples and for both the $^4F_{9/2}$ and $^4S_{3/2}$ levels the decay times lengthen as the temperature is decreased. However, there is a difference in the behavior of the decay times for the bulk and nanocrystalline samples as a function of temperature. For the bulk sample, the $^4S_{3/2}$ level decays more rapidly on increasing the temperature with respect to the $^4F_{9/2}$ level, which is different from the nanocrystalline sample in which this different behavior is not observed (see Table 2). The observed rate of depopulation W of an excited state could be expressed as the sum of the radiative W_R and multiphonon transition probabilities W_{MPR}. While W_R is independent of the temperature for a transition between $4f^n$ states, the dependence of W_{MPR} from the temperature could be written as[7]

$$W_{MPR}(T) = W_{MPR}(0)(1 + n_{eff})^p \quad (4)$$

where

$$n_{eff} = [\exp(\hbar\omega_{eff}/kT) - 1]^{-1} \quad (5)$$

is the occupancy of the effective phonon mode of energy ($\hbar\omega_{eff}$) and p is the number of phonons necessary to bridge the energy gap between the emitting level and the next lower level. According to eq 4, W would increase and therefore the observed decay time $\tau = W^{-1}$ would decrease upon raising the temperature. If we consider the energy gap between the $^4S_{3/2}$ and $^4F_{9/2}$ levels to be about 3000 cm^{-1} and thus allow five maximum energy phonons to participate in the nonradiative relaxation, then the variation in the decay time of the $^4S_{3/2}$ level is not well explained by eq 4 alone. In fact, the thermalization of the $^2H_{11/2}$ level by the $^4S_{3/2}$ level is also involved in determining the observed behavior of the decay times, as the radiative lifetime of the upper-lying state ($^2H_{11/2}$) is distinctly shorter than the one of the lower level ($^4S_{3/2}$).[29] Therefore, it is expected that the lowering of the temperature induces the depopulation of the short-lived $^2H_{11/2}$ level and consequently an increase of the observed decay time. In the present case, both mechanisms are active; the relatively high number of phonons required for the multiphonon relaxation probably makes the thermalization process more important.

Also of note is the variation, with temperature, of the emission from the $^4F_{9/2}$ level. On passing from room to lower temperature, the $^4F_{9/2}$ level is populated by a weaker multiphonon relaxation from the $^4S_{3/2}$ level above. Since the energy gap between the $^4F_{9/2}$ level and the next lower $^4I_{9/2}$ level is about 2500 cm^{-1}, and if the intrinsic decay rate of the $^4F_{9/2}$ is higher than that of the thermalized $^4S_{3/2}$ level, then the multiphonon relaxation from the $^4S_{3/2}$ level will be the bottleneck, causing the decay times from both levels to be identical. The longer observed decay time from the $^4F_{9/2}$ level may reflect a weaker decay rate from this level.

4. Conclusions

We have reported and discussed NIR to visible upconversion in bulk and nanocrystalline $Lu_{1.98}Er_{0.02}O_3$ following 980 nm continuous wave excitation. The upconverted luminescence intensity for the nanocrystalline sample was lower than its bulk counterpart owing to a higher probability of multiphonon relaxation because of the adsorbed CO_2 and H_2O on its surface. Power studies revealed that the green ($^4S_{3/2} \rightarrow {}^4I_{15/2}$) and red ($^4F_{9/2} \rightarrow {}^4I_{15/2}$) upconversion occurred via a two-photon process. The electronic energy level of the Er^{3+} ion possesses a level at exactly twice the excitation energy ($^4F_{7/2}$) and therefore, upconversion will occur via an excited-state absorption (ESA) process. However, lifetime measurements also showed that energy-transfer upconversion (ETU) will occur as the lifetime of both green- and red-emitting levels are longer when exciting with 980 nm compared to direct excitation with 488 nm.

Blue upconversion was observed, assigned to the $^4F_{5/2} \rightarrow {}^4I_{15/2}$, $^2P_{3/2} \rightarrow {}^4I_{11/2}$, and $^4F_{7/2} \rightarrow {}^4I_{15/2}$ transitions. A power study revealed that the $^2P_{3/2}$ emitting level was populated via a three-photon process. Population of the $^2P_{3/2}$ level via an ESA process is improbable as no resonance exists for a process involving the sequential absorption of three photons. Therefore, an ETU mechanism assisted by phonons was determined to be operative.

The natural extension of this work is to study the dynamics of the upconversion process. Further experiments using pulsed excitation are currently in progress and will be the subject of a future paper.

Acknowledgment. The authors gratefully thank Erica Viviani (Università di Verona, Italy) for expert technical assistance and Stefano Polizzi (Università di Venezia, Italy) for the X-ray measurements on nanocrystalline $Lu_{1.98}Er_{0.02}O_3$. The authors acknowledge the Natural Science and Engineering Research Council of Canada and MURST (project 9903222581_005) of Italy for financial support.

References and Notes

(1) Dieke, G. H. *Spectra and Energy Levels of Rare Earth Ions in Crystals*; Interscience Publishers: New York, 1968.
(2) Hüfner, S. *Optical Spectra of Transparent Rare Earth Compounds*; Academic Press: New York, 1978.
(3) Tissue, B. M. *Chem. Mater.* **1998**, *10*, 2837−2845.
(4) Goldburt, E. T.; Kulkarni, B.; Bhargava, R. N.; Taylor, J.; Libera, M. *J. Lumin.* **1997**, *72−74*, 190−192.
(5) Scheps, R. *Prog. Quantum Electron.* **1996**, *20*, 271−358.
(6) Capobianco, J. A.; Prevost, G.; Proulx, P. P.; Kabro, P.; Bettinelli, M. *Opt. Mater.* **1996**, *6*, 175−184.
(7) Riseberg, L. A.; Moos, H. W. *Phys. Rev.* **1968**, *174*, 429−438.
(8) Capobianco, J. A.; Vetrone, F.; Boyer, J. C.; Speghini, A.; Bettinelli, M. *Opt. Mater.* **2002**, *19*, 259−268.
(9) Wyckoff, R. W. G. *Crystal Structures;* 2nd ed.; Interscience: New York, 1964; Vol. 2.
(10) Saiki, A.; Ishizawa, N.; Mizutani, N.; Kato, M. *J. Ceram. Soc. Jpn.* **1985**, *93*, 649−654.
(11) Forest, H.; Ban, G. *J. Electrochem. Soc.* **1969**, *116*, 474−478.
(12) Tessari, G.; Bettinelli, M.; Speghini, A.; Ajò, D.; Pozza, G.; Depero, L. E.; Allieri, B.; Sangaletti, L. *Appl. Surf. Sci.* **1999**, *144−145*, 686−689.
(13) Ye, T.; Guiwen, Z.; Weiping, Z.; Shangda, X. *Mater. Res. Bull.* **1997**, *32*, 501−506.
(14) Capobianco, J. A.; Vetrone, F.; Boyer, J. C.; Speghini, A.; Bettinelli, M. *J. Phys. Chem. B* **2002**, *106*, 1181−1187.
(15) Maunier, C.; Doualan, J. L.; Moncorgé, R.; Speghini, A.; Bettinelli, M.; Cavalli, E. In *Trends in Optics and Photonics*; Marshall, C., Ed.; Proceedings of Advanced Solid-State Lasers, Vol. 50; Optical Society of America: Seattle, WA, 2001; pp 261−264.
(16) Rambaldi, P.; Moncorgé, R.; Wolf, J. P.; Pédrini, C.; Gesland, J. Y. *Opt. Commun.* **1998**, *146*, 163−166.
(17) Guillot-Noël, O.; Bellamy, B.; Viana, B.; Vivien, D. *Phys. Rev. B* **1999**, *60*, 1668−1677.
(18) Moine, B.; Dujardin, C.; Lautesse, H.; Pedrini, C.; Combes, C. M.; Belski, A.; Martin, P.; Gesland, J. Y. *Mater. Sci. Forum* **1997**, *239−241*, 245−248.
(19) Bloembergen, N. *Phys. Rev. Lett.* **1959**, *2*, 84−85.
(20) Chivian, J. S.; Case, W. E.; Eden, D. D. *Appl. Phys. Lett.* **1979**, *35*, 124−125.
(21) Auzel, F. *C. R. Acad. Sci. (Paris)* **1966**, *262*, 1016−1019.

(22) Joubert, M. F.; Guy, S.; Jacquier, B. *Phys. Rev. B* **1993**, *48*, 10031−10037.

(23) van der Ziel, J. P.; Ostermayer, F. W.; Van Uitert, L. G. *Phys. Rev. B* **1970**, *2*, 4432−4441.

(24) Capobianco, J. A.; Raspa, N.; Monteil, A.; Malinowski, M. *J. Phys.: Condens. Matter* **1993**, *5*, 6083−6090.

(25) Shinn, M. D.; Sibley, W. A.; Drexhage, M. G.; Brown, R. N. *Phys. Rev. B* **1983**, *27*, 6635−6648.

(26) Meltzer, R. S.; Feofilov, S. P.; Tissue, B.; Yuan, H. B. *Phys. Rev. B* **1999**, *60*, 14012−14015.

(27) Garcia-Murillo, A.; Le Luyer, C.; Pedrini, C.; Mugnier, J. *J. Alloys Compd.* **2001**, *323*, 74−77.

(28) Medenbach, O.; Dettmar, D.; Shannon, R. D.; Fischer, R. X.; Yen, W. M. *J. Opt. A: Pure Appl. Opt.* **2001**, *3*, 174−177.

(29) Weber, M. J. *Phys. Rev.* **1968**, *171*, 283−291.